Eur. Phys. J. B **30**, 265–274 (2002)
DOI: 10.1140/epjb/e2002-00378-3

THE EUROPEAN PHYSICAL JOURNAL B

Numerical simulation and experiments of a control method to suppress the Bénard von Kármán instability

R.H. Hernández[a] and A. Pacheco

LEAF-NL, Departamento de Ingeniería Mecánica Universidad de Chile, Casilla 2777, Santiago, Chile

Received 7 March 2002 / Received in final form 12 September 2002
Published online 29 November 2002 –

Abstract. We report both two-dimensional numerical simulations and experimental results that confirm the robustness of a new method for inhibiting vortex shedding associated to the Bénard–von Kármán (BvK) instability in the wake of a cylinder. Using the SIMPLER algorithm on a 2D channel, we solve the Navier-Stokes equations and we show that pressure suction at the front stagnation point of a circular cylinder, modelled here through a point sink located at the front stagnation point, can completely suppress the Bénard–von Kármán instability for super-critical Reynolds numbers. Comparison with recent experimental results are in close agreement.

PACS. 47.27.Vf Wakes – 47.20.-k Hydrodynamic stability – 47.27.Rc Turbulence control

Introduction

Instabilities in non linear systems driven far from equilibrium often consist of transitions from motionless states to one varying periodically in space or time. Actually a lot of beautiful examples have become very popular, like Rayleigh–Bénard convection, waves in shear flows, Couette–Taylor flow, oscillatory chemical reactions and the well known Bénard von Kármán (BvK) instability.

The onset of periodic structures in these systems when driven by spatially homogeneous or time constant forcing, corresponds typically to a bifurcation, characterized by one or several modes that become unstable. In particular, pattern forming instabilities of vortical nature, such the Bénard–von Kármán (BvK) instability can induce a phenomenon which generates strong transverse force fluctuations originated by the periodic vortex shedding from bluff bodies. The BvK instability can be generated in the wake of a circular cylinder of diameter d and length L, and it is commonly accepted that for large aspect ratios, $\Gamma = L/d \gg 1$, the onset for vortex shedding occurs for a critical value of the Reynolds number ($Re = U_o d/\nu$, where U_o, ν are the kinematic viscosity and mean fluid velocity respectively) close to $Re_c \sim 50$ [1,2]. At low Reynolds numbers, of order one, a reversed flow first occurs near the rear stagnation point of the cylinder and leads to the formation of two attached eddies in the near wake of the cylinder, thus breaking the upstream-downstream symmetry. The two attached eddies grow in size as the Reynolds number is increased, and at a Reynolds number close to the threshold $Re \sim Re_c$, the flow ceases to be symmetric about the centerline and stationary; it settles into a time periodic regime in which vortices are shed alternatively from the two sides of the cylinder, giving rise to the von Kármán vortex street [3]. Vortex shedding corresponds to a limit–cycle oscillation of the near wake described by a Stuart–Landau equation [1].

Controlling the wake of a cylinder by inhibiting the BvK instability has motivated a lot of studies. Two forms of wake control are currently proposed in the literature, called respectively active or passive methods. In the group of passive methods, inserting a splitter plate in the near wake of a cylinder [4], performing steady or periodic suction from the rear circulation zone [5], heating the cylinder, locating a secondary cylinder in the near wake, imposing large–amplitude transverse oscillations or angular rotation to the cylinder at an appropriate frequency, can at least modify or suppress vortex shedding [6–8]. In the group of active methods, an electronic feedback is achieved with the aid of a pressure (or velocity) sensor, by applying for instance acoustic forcing [9,10] or using a pair of blowing–suction actuators near the circulation region [9].

Most of the above methods, active or passive, have tried to control the BvK instability by applying a local perturbation directly in the near wake of the cylinder. This is a quite natural idea if we have in mind the methods used to control boundary layer separation by trying to inhibit adverse pressure gradients along the trailing edge of solid bodies in a flow field. Another concept that may be invoked to justify a perturbation directly applied to the wake is the one of absolute versus convective instability [11]. Perturbing the wake, for instance using a blowing actuator at the rear stagnation point, one may hope to

[a] e-mail: rohernan@cec.uchile.cl

transform an absolute instability of the near wake into a convective one.

The control method here analyzed [12] differs from the ones mentioned above. We look for a global modification of the flow field around the cylinder changing its pressure distribution. Normally, the average pressure in the near wake is smaller than the one near the front stagnation point. This difference with the potential flow solution, is due to boundary layer separation that generates a vorticity filled wake in which the pressure is low. The general idea, as expressed in [12] is thus to compensate this pressure difference by decreasing the pressure at the front stagnation point, say $p_f(t)$. This was achieved through a local suction, which in turn decreases the average local pressure near that point. The front stagnation point is thus suppressed and bifurcates into a pair of stagnation points located symmetrically with respect to the flow centerline, at angles $\pm\theta_o$, and shifted downstream as the amount of suction is increased. We have shown using potential flow theory, that this modifies the pressure distribution around the whole cylinder such that the streamlines shrink in the wake of the cylinder. This externally imposed asymmetry is thus likely to compensate the one which results from boundary layer separation and consequently to delay the onset of the BvK instability.

Using the control volume formulation and an iterative semi-implicit scheme [13] on a 2D equally spaced grid, we solve the time varying Navier Stokes equations on a rectangular channel with a circular cylinder inside. The control method is formulated as close as possible with the experiments, incorporating a local sink of strength Q at the front stagnation point of the cylinder.

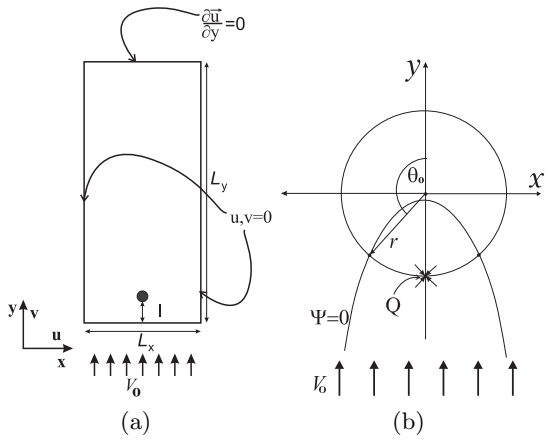

Fig. 1. (a) Physical configuration. A 2D channel of dimensions $(L_x, L_y) = (16d, 30d)$, discretized with a grid of 321×601 points, where a cylinder of diameter d is located near the channel's entrance at $l = 2d$. (b) Schematic theoretical prediction from potential theory of the bifurcated position, θ_o, for two new symmetric stagnation points, when a sink of strength Q is located at position (r, π). Singular stream function $\Psi = 0$ is also shown.

Formulation

Problem description

The physical situation in Figure 1a, corresponds to a rectangular channel of aspect ratio $L_y/L_x = 1.87$. A circular cylinder of diameter d, located two diameters apart from the channel entrance, is simulated through the block-off procedure for irregular geometries [13]. The 2D governing equations for fluid velocity (u, v) and pressure p, retaining their time derivatives in dimensionless form and index notation are,

$$\frac{\partial u_i}{\partial x_i} = 0 \tag{1}$$

$$\frac{\partial u_i}{\partial t} + u_j \frac{\partial u_i}{\partial x_j} = -\frac{\partial p}{\partial x_i} + \frac{1}{Re_x}\nabla^2 u_i. \tag{2}$$

The channel Reynolds number is defined as $Re_x = v_0 L_x/\nu$, where v_0, ν are the streamwise velocity at the channel entrance and the kinematic viscosity respectively. The cylinder based Reynolds number is $Re = Re_x(d/L_x)$. Variables like time, velocity, pressure were scaled using v_0/L_x, $1/v_0$, ρv_0^2, as reference quantities respectively, where ρ is the fluid density. The Cartesian coordinates are scaled with the transverse channel size L_x, and reference axes are such that streamwise direction is y (v velocity) and transverse direction is x (u velocity). Governing equations were solved with our code in primitive variables using the finite volume formulation and the SIMPLER algorithm [13–15]. Discretization of the physical domain incorporates a two–dimensional, uniform and staggered grid of 321×601 points. Fluid velocity vanishes on rigid walls and Newmann conditions are imposed at the channel's exit. Boundary conditions for fluid velocity in non dimensional form (u, v) are the following:

$$y = 0 \quad (0 \le x \le L_x) \rightarrow \quad [u = 0, v = 1] \tag{3}$$

$$y = L_y \quad (0 \le x \le L_x) \rightarrow \left[\frac{\partial u}{\partial y} = 0, \frac{\partial v}{\partial y} = 0\right] \tag{4}$$

$$x = 0, L_x \quad (0 \le y \le L_y) \rightarrow \quad [u = 0, v = 0]. \tag{5}$$

Spatial and time steps of $\delta x = \delta y = 3.125 \times 10^{-3}$ and $\delta t = 10^{-3}$ respectively, give both grid independent solutions and enough resolution for the wavy behavior (vortex shedding) of the developing BvK instability.

Control method

Theoretical solution for the flow potential $\phi(r)$ originated by a local sink of strength Q in two dimensions, satisfies the Laplace equation $\nabla^2\phi = 0$ and the overall velocity field $\mathbf{v} = -\nabla\phi$ decays typically as $1/r$. where $r = |\mathbf{r}|$ is the distance from sink. Its influence on the physical domain is considerably stronger than equivalent solution in three dimensions, where velocity decreases as $1/r^2$.

The two dimensional form of a local sink is the key of our control method. In our 2D numerical runs, the control method is mathematically modelled incorporating a point sink of strength Q at the cylinder surface exactly were the front stagnation point occurs (see Fig. 1). Numerically, we impose a local sink of strength Q in the governing equations, through the source terms arising from the discretized equations, in particular from the mass conservation equation [16]. The sink is imposed only at the front stagnation point of the cylinder, *i.e.*, only over one grid point.

An inviscid model of the 2D flow field around a circular cylinder with a sink located at the front stagnation point has been drawn from potential theory. Details of the theoretical calculations can be found in [12]. As a result, the steady state solution of the stream function for a given sink strength Q shows that the front stagnation point is suppressed and bifurcates into a pair of stagnation points located symmetrically with respect to the flow centerline, at angles $\pm\theta_o$, and shifted downstream as the amount of suction is increased (see Fig. 1). The theoretical solution, as shown in [12], can be expressed as

$$\theta_o = \arccos\left(\frac{Q}{4\pi d v_0} - 1\right).$$

These new stagnation points can be found from our numerical solutions, by looking for local maxima of surface pressure at the cylinder surface [16]. Our local sink model was compared to the inviscid theory through the contours map for the stream function $\Psi(x, y)$ in two dimensions. Overall flow solutions were found for the steady state velocity field generated by a local (point-like) sink interacting with a uniform and parallel velocity flow v_0 imposed at the channel's entrance (without cylinder). These numerical results (not shown here), in very close agreement with the potential solution, where used as test solutions of grid spacing for the numerical code [16].

We will see that, as predicted by potential theory [12,16], if we operate the complete model; sink + cylinder, at Reynolds numbers greater than the critical value, $Re \geq Re_c$, ($Re_c \sim 50$) we found that, both the bifurcation phenomena associated to the new stagnation points really occurs and if the sink strength is greater than a critical value ($Q > Q_c$), vortex shedding suppression takes place, inhibiting the BvK instability.

Results

Natural BvK instability

The choice of the channel aspect ratio, cylinder size, and grid size were found computing the overall solution for Reynolds numbers Re below and above the critical one Re_c. Stable and unstable states of the system can be detected recording the transverse fluid velocity $u(t)$ some diameters apart downstream the cylinder. The monitoring point (or sensor's location) is located at the middle of the channel but can take different streamwise y positions (measured in cylinder diameters) downstream the body.

Our choice to validate the code has been to compute the characteristic eigen values associated to the IBvK instability for different Reynolds numbers. For short times after instability onset, linear theory predicts that instability will occur when the most unstable mode, $\sigma = \sigma_r + j\omega$, crosses the imaginary axis, *i.e.*, when $\sigma_r > 0$. The associated frequency ω is not zero, as proved in [1,2], which corresponds to a Hopf bifurcation. These runs are very time consuming, because as we approach the instability threshold, the characteristic growth rate scales as $\tau = \sigma_r^{-1} \sim (Re - Re_c)^{-1}$ and one must wait very long times (long transients) to record an acceptable evolution, in this case, of $u(t)$.

To obtain these parameters in our simulation, we imposed a impulsive starting flow around the circular cylinder and then solve the full Navier-Stokes equations. As in experiments, the impulsive starting flow is an appropriate way to excite the system. Numerically we impose a step function for the channel entrance flow velocity as $v_0(t) = v_0\Theta(t)$, where $\Theta(t)$ is the Heavise step function.

The system response ($u(t)$) for short times is of exponential form, $u(t) \sim \mathrm{e}^{\sigma t}$ and both envelopes and instantaneous frequency, can be easily computed using the analytic signal representation of $u(t)$, as explained in the next section.

These results are shown in Figure 2. The evolution of the characteristic shedding frequency ω is plotted in the form of Roshko number, $Ro = fd^2/\nu$, where $f = \omega/2\pi$, as a function of Reynolds number (Fig. 2a). The sub-critical and super-critical regimes follow a linear relationship, but display a different slope. The slope ratio found is

$$\Gamma = \frac{\Delta_{\sigma_r<0}}{\Delta_{\sigma_r>0}} = 0.74$$

where $\Delta_{\sigma<0}, \Delta_{\sigma>0}$ are the slopes for the sub-critical and super-critical curves respectively. This value can be also computed from a recent experimental work [2] where a very close agreement is found.

Figure 2b shows the corresponding growth rates for the sub-critical ($\sigma_r < 0$) and super-critical ($\sigma_r > 0$) regions. A linear evolution with Reynolds number is found as predicted by Landau theory. The critical Reynolds number can be obtained by extrapolation, $\sigma_r \to 0$, from both sides. Critical values are $Re_c(\sigma_r < 0) = 57.4$ and $Re_c(\sigma_r > 0) = 56.8$, differing in 1 %, uncertainty associated to the accuracy of logarithmic linear fit over the exponential part of the envelope of transverse velocity.

These critical Reynolds numbers are slightly higher than the common value $Re \sim 50$ [1,2], indicating that blockage effects associated to our channel dimensions are not negligible. Blockage effects are such that reducing the ratio L_x/d will rise the critical value, Re_c, associated to the onset of the BvK instability. To determine a limiting critical Reynolds number, one can consider a blockage correction procedure, computing systematically Re_c as a function of the ratio d/L_x and then extrapolate to $d/L_x \to 0$, but this is far beyond the scope of this work.

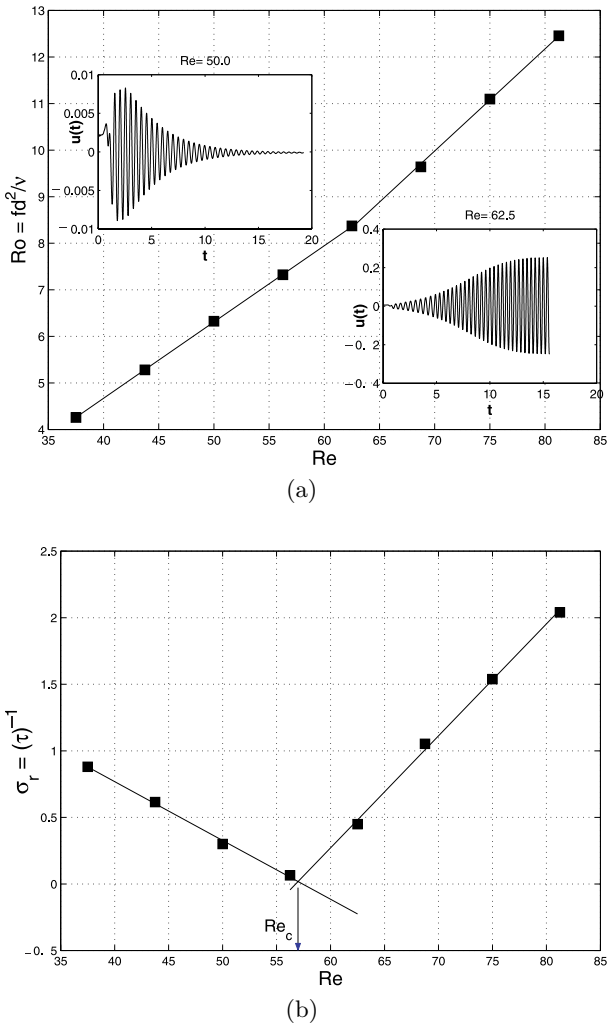

Fig. 2. Typical parameters obtained for the BvK instability for impulsive starting flow around the circular cylinder. (a) The Roshko, $Ro = fd^2/\nu$, number as a function of Reynolds number, Re, for the sub-critical and super-critical regions. Two different slopes occur for the best fit between shedding frequency and Reynolds number. We show two sub-plots for typical stable and unstable eigen modes, through the transverse component of fluid velocity. (b) Corresponding characteristic stable and unstable growth rates τ as a function of Reynolds number Re. The arrow indicates critical Reynolds number $Re_c \sim 58$.

A closer look of the time evolution of the pattern forming instability is shown in Figure 3, where we plot a sequence of vorticity contours, $\boldsymbol{\omega} = \nabla \times \mathbf{v}$, corresponding to a single time period (the inverse of the Strohual frequency) of the characteristic vortex shedding at $Re = 100$. Here we see an alternate shedding of local regions of intense vorticity which are characteristic of the BvK instability. These high vorticity regions, of opposite circulation, are advected by the mean flow and leave the computational domain without any deformation, which assures us on the right use of Newmann boundary conditions at the channel's exit. The reader should note that

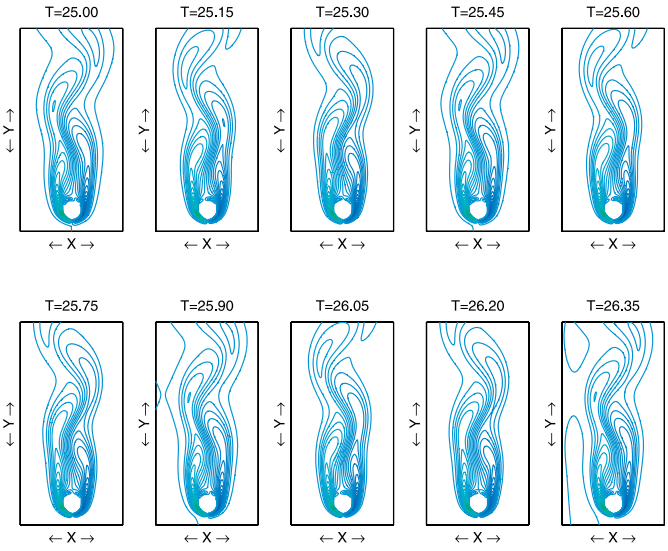

Fig. 3. Single period of vortex shedding in the form wake vorticity $\boldsymbol{\omega} = \nabla \times \mathbf{v}$ contours at Reynolds number $Re = 100$.

another signature of the BvK instability is that, increasing the Reynolds number produce a decrease of the characteristic wavelength, λ_ω, associated to the wavy pattern (Strouhal frequency increases) as it is documented on different experiments [17–19].

Controlling BvK instability

Now, in order to suppress vortex shedding at a given Reynolds number, $Re > Re_c$, we should start the control method; this is done turning on the local sink at the front stagnation point of the cylinder. Prior to that, we must be careful and find the final periodic flow field obtained at the working Reynolds number, say at $t = t_0$. After that, the sink is activated through a time (τ_v) limited step function, *i.e.*, $Q(t) = Q\,\Theta(t)$, where,

$$\Theta(t) = \begin{cases} 1, & \text{if } t_0 < t < (t_0 + \tau_v) \\ 0, & \text{otherwise} \end{cases}$$

The result is clearly seen in Figure 4. At $Re = 100$, after the instability attained its saturated regime, which consist of a constant amplitude periodic oscillating flow field, the sink is turned on abruptly following the step function indicated above. Seven sink strength values were used, ranging from $Q = 0.04 \rightarrow 0.1$. For this case, when $Q > 0.04$ the flow field becomes stable during the sink on-operation. During that period of time, denoted as τ_v, the BvK instability displays a similar behavior. At first, when the sink is started, the instability is damped and its associated vortex shedding is being suppressed. To make the point, we plot the signal corresponding to the transverse fluid velocity $u(t)$, which displays that characteristic damping, which was found to depend on the sink strength. The higher Q the shorter is the characteristic time, as we see if we compare the oscillating patterns. This fact implies that the original eigen value spectrum for $Re = 100$

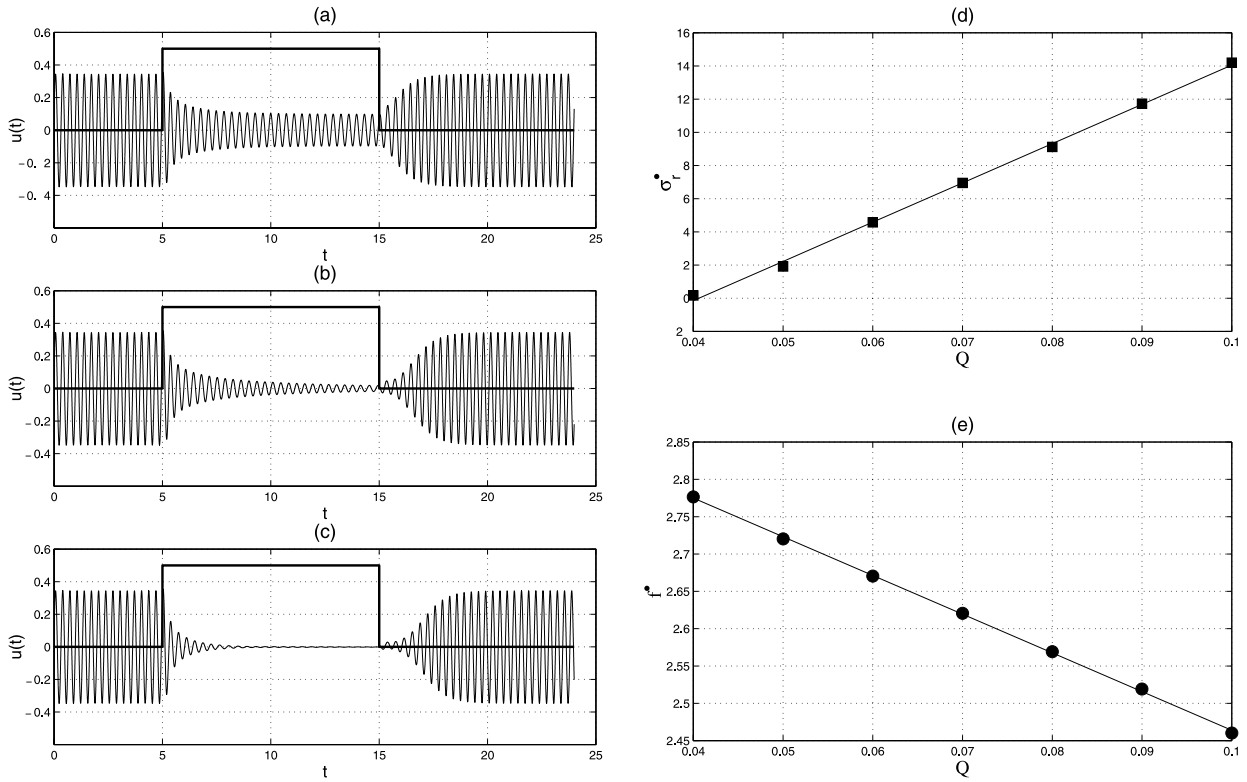

Fig. 4. Wake behavior of the transverse rms fluid velocity $u(t)$ at 2 diameters downstream the cylinder end. These signals are found when the BvK instability is virtually modulated by an on-off operation of the local sink. The on-off operation of the sink is shown here as a TTL or square signal for $t \in [5, 15]$. (a) $Re = 100$, $Q = 0.04$ (b) $Re = 100$ $Q = 0.05$, (c) $Re = 100$, $Q = 0.07$. At constant Re, as the sink strength Q increases, the unstable mode becomes stable. (d) A characteristic growth rate associated to new eigen values, $\sigma_r^\bullet$, show that a critical Q exists, and (e) if Q increases, the associated new shedding frequency $f^\bullet$ is found to decrease.

has moved to the left part of the complex plane (σ_r, ω) such that $\sigma_r < 0$. We must recall that the effect is an overall one, *i.e.*, the instability is really suppressed at any location on the computational domain. There exists however a time lag between the switching of the step and what it is measured at the monitoring point. This effect is explained because the oscillating pattern is always advected by the mean flow [3].

It is clear that the effect of the local sink is to suppress the developing instability, however there exists a critical sink strength, Q_c, over which the BvK instability is well damped. As it was shown in a previous experimental work [12], for each given super-critical Reynolds number, there is associated a critical strength. If $Q > Q_c$ the control method works fine, however Q_c seems to increase with the value of Re. In our case, the determination of critical Q_c values is not simple. To look for a critical Q_c value, we must run our numerical simulation for a constant Re value, recording the wake velocity in time. Starting with an arbitrary value of $Q < Q_c$, we increase Q in small steps until the characteristic oscillatory velocity signal dies out. Figure 5a shows the time recording of this situation. Varying Q between the interval $[0.01, 0.06]$ at $Re = 100$ we observe a systematic decrease of the amplitude of wake fluctuating transverse velocity, $u(t)$. The effect is appreciated over the two components of the wake velocity. The effect on the streamwise velocity component is dependent on the sensor position. An increase of $v(t)$ is found at one diameter $(1d)$ from the cylinder end, however a net decrease at $2d$, $4d$ and $8d$ is observed. The near wake shows an increase in the average streamwise fluid velocity, $v(t)$, due to the local acceleration created by the shrink of the stream lines near the cylinder end, so the wake's streamwise velocity must increase, as it is observed. However far from the cylinder, the overall wake carries less fluid as we have pumped a certain quantity with the sink. So, the average flow rate decreases, and consequently the streamwise mean velocity.

An accurate criteria, on the transverse fluid velocity, was used to proceed to increase or to decrease the sink strength in small steps, $\delta Q \sim 0.01$. We computed the envelope of $u(t)$ at the monitoring point, using a Hilbert transform to create and analytic signal [20] of the real one $u(t)$. This can be done as follows,

$$u_a(t) = u(t) + j \cdot \mathcal{H}[u(t)]$$

where,

$$\mathcal{H}[u(t)] = VP\frac{1}{\pi}\int_{-\infty}^{\infty} \frac{u(t')}{t - t'}\,\mathrm{d}t'$$

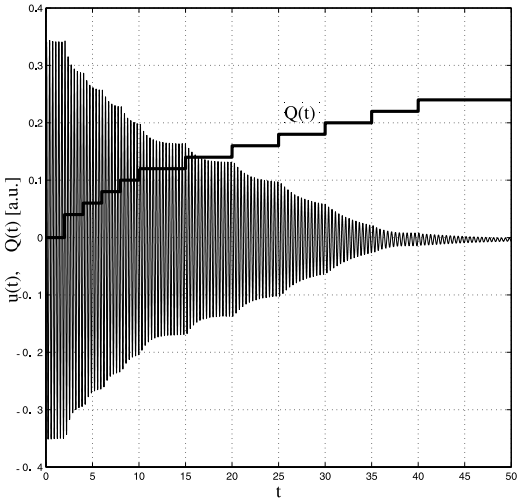

(a)

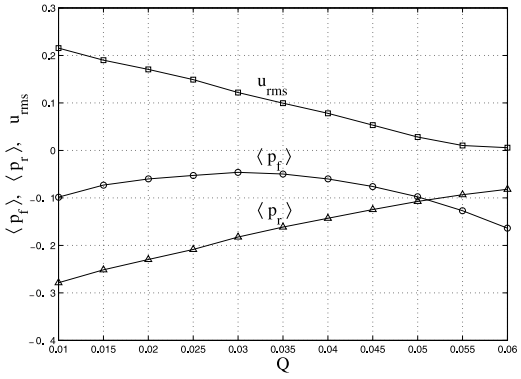

(b)

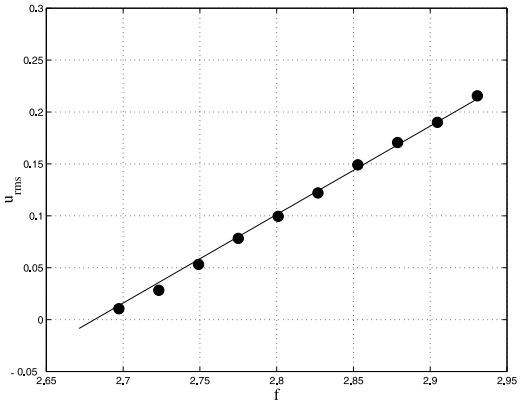

(c)

Fig. 5. The effect of increasing sink strength Q on the wake velocity at $Re = 100$. Sink strength Q varies from $Q = 0.01$ to $Q = 0.06$. (a) Time series for the transverse component of fluid velocity, $u(t)$ at $(x, y) = (0.5, 0.5)$ *versus* time for each value of sink strength Q. (b) Evolution of rms transverse velocity, u_{rms}, and averaged pressure at the front, $\langle p_f \rangle$, and rear, $\langle p_r \rangle$, points at the cylinder surface with sink strength Q. (c) Evolution of saturated amplitude u_{rms} corresponding to the r.m.s final value of fluid velocity $u(t)$ *versus* shedding frequency f.

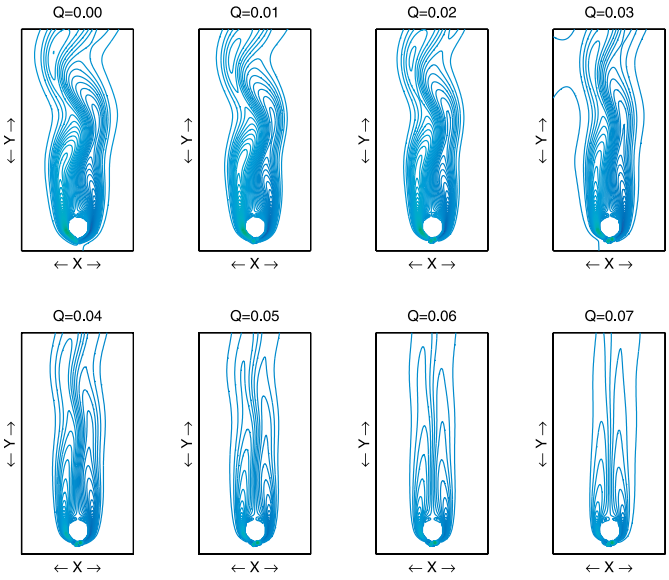

Fig. 6. Wake vorticity $\boldsymbol{\omega} = \nabla \times \mathbf{v}$ contours at Reynolds number $Re = 100$ when the sink strength Q is increased in steps $\delta Q = 0.01$. Note here the systematic increase of characteristic wavelength of vortex pattern.

is the Hilbert transform of the real signal $u(t)$. We impose the slope of $|u_a(t)|$ should be less than a small value to increase the sink strength in another step.

$$\frac{\mathrm{d}|u_a(t)|}{\mathrm{d}t} \leq 10^{-3}.$$

The advantage of this complex signal is that we get both the instantaneous signal envelope as $|u_a(t)|$ and frequency as $f = \frac{1}{2\pi}\frac{\mathrm{d}\varphi}{\mathrm{d}t}$ at the same time (φ is the phase of $u_a(t)$).

With this criteria, starting form the saturated regime at $Re = 100$, we performed a continuous cycle for the sink strength, first increasing and then decreasing it to look for an expected hysteresis on $u(t)$ amplitude.

Hysteresis is not found, *i.e*, both the evolution of $|u_a(t)|$ amplitude, as well as the shedding frequency, f, do not depend on the sense (increase/decrease) of the forcing cycle for Q.

Role of Q on saturated properties

In Figure 5b we show the evolution of the time-averaged values of local pressure $\langle p_f \rangle$ and $\langle p_r \rangle$ with sink strength, both at the front, $p_f(t)$, and rear, $p_r(t)$, stagnation points respectively on the cylinder surface.

When $\langle p_f \rangle \sim \langle p_r \rangle$ we found that the r.m.s. velocity fluctuation u_{rms} approaches to zero (fall into numerical background noise), which confirms that it is the average pressure balance that brings back a kind of flow symmetry, upstream-downstream, found at very low Reynolds numbers (*e.g.*, Stoke's flow).

A more rigorous calculation would be to consider the evolution of a time-averaged pressure coefficient C_p at the cylinder surface, to compare them with potential flow solution for example. But it is too time consuming and goes

beyond the global explanation of shedding inhibition of this work.

The evolution of rms velocity fluctuations u_{rms} with shedding frequency f is shown in Figure 5c. The saturated amplitude corresponding to the $u(t)$ fluctuations decreases with increasing Q, as shown in Figure 5b, showing clearly the presence of a critical value, $Q = Q_c$, where fluctuations fall into the numerical background noise. The critical value found here is approximately $Q_c \sim 0.05$, as can be guessed in Figure 4d. The fact is that switching the sink on, $Q \neq 0$, at a given Re, modifies both the shedding frequency, f (reduces it) and the real part of the most unstable eigen value, σ_r. See for instance Figure 4e and also Figure 5c. The effect can be viewed as if we locally reduce the Re number, bringing back the flow stable.

A closer look of the wake behavior using the control method is shown in Figure 6. We show the wake vorticity contours as a function of the sink strength values between $0 \leq Q \leq Q_c$. As we observe, increasing the sink strength results in a efficient vortex shedding suppression. The BvK instability has been inhibited. The evident decrease of velocity fluctuations as well as, of the characteristic shedding frequency or Strouhal frequency, are associated with an increase of the wavelength of the BvK wavy wake. In general, this way of control allows a fine *tunning* of the characteristic frequency and wavelength of the instability, simply by adjusting the sink strength.

The mechanism, as we pointed out before, by which the vortex shedding is suppressed, is deeply related to the bifurcation of the original stagnation point into two points located symmetrically with respect to the flow centerline, at angles $\pm\theta_o$. These new points can be shifted downstream if the sink strength is increased.

These new stagnation points appear as a consequence of the deflected fluid path produced by the active sink. The overall effect of the method is to achieve a global modification of the flow field around the cylinder, specially changing its pressure distribution. For the unforced case, the average pressure in the near wake is smaller than the one near the front stagnation point, and the role of the sink is to compensate this pressure difference by decreasing the pressure at the front stagnation. If the pressure field is reinforced, the adverse pressure gradient is reduced, boundary layer separation does not occur, vortex shedding is suppressed and the cylinder's wake recovers its transverse symmetry.

Comparison with some experiments

Numerical results were compared with recent experiments developed at our laboratory, concerning the nature of the BvK instability. Experiments were conducted in a closed loop air wind tunnel. The wind tunnel supports two laminarization chambers built on aluminium honey comb panels (nominal diameter 6.35 mm) placed before each of the two test sections. The turbulence level, defined as the ratio of the rms velocity to the average flow velocity, does not exceed 0.5 % with accuracy better than ±1% on mean velocity. The BvK instability is triggered over a vertically aligned long-span circular cylinder ($d = 4.0 \pm 0.1$ mm, $L = 17.5 \pm 0.1$ cm), mounted at the main 50×50 cm (low velocity) test section (Fig. 7). Two fine metallic end-disks were attached to the cylinder ends, in order to avoid the presence of other shedding modes [21].

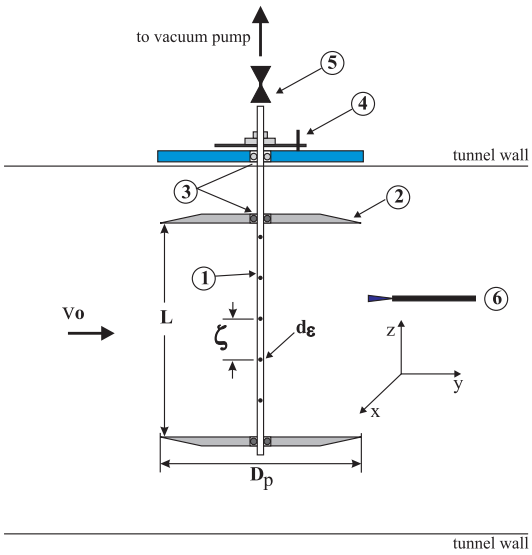

Fig. 7. Schematics of the experimental set up at the wind tunnel test section. The wind tunnel facility consists of a closed loop air wind tunnel with two test sections: a small one of 20×20 cm, and bigger one of 50×50 cm. A wide range of flow velocities is possible with two independent groups of fans: one for low velocities using 16 axial DC fans ($10 - 200$ cm/s) and one centrifugal blower for higher velocities ($2-20$ m/s). (1) The circular cylinder (diameter $d = 4$ mm, $L = 17.5$ cm) showing the small hole distribution with $\zeta/d = 3.75$ and $d_\epsilon = 0.5$ mm. It is bounded by two end-plates ($D_p/d = 10$)(2) and mounted on small ball bearings (3). Outside the wind tunnel wall an accurate goniometer (4) is used to determine angle between small holes and the streamwise flow velocity v_0. Cylinder's top end joins a vacuum pump through (5) a rapid (up 100 Hz) solenoid valve. Fluid velocity is measured with a hot wire probe (6) at $y/d = 18$.

As in [12], to decrease the pressure at the front stagnation point, $p_f(t)$, we have drilled a very small hole of diameter d_ϵ ($d_\epsilon/d \ll 1$) to connect the surface of the tube to its inner section, which is connected to an external vacuum pump, as shown in Figure 7. To get an overall effect along the cylinder span L, we drilled an uniform distribution of 11 very small holes ($d_\epsilon = 0.5$ mm) along a straight line at the cylinder's surface. A step size of $\zeta/d \sim 3.75$ between the holes was used. We have chosen a discrete hole distribution instead of a continuous slit because pressure modulation would not have been possible due to the limited power of the vacuum network at our disposal (21 m^3/hr).

To perform fast pressure changes at the stagnation point, the vacuum network is connected through a rapid solenoid valve. The operating local strength, Q in cm^3/s, for the whole sink distribution at the cylinder's surface is fixed with a flow meter. For rapid pressure changes a solenoid on–off valve was triggered with a square TTL signal. Flow rates Q were measured with a calibrated flow meter Dwyer VFB series, and can be normalized by a

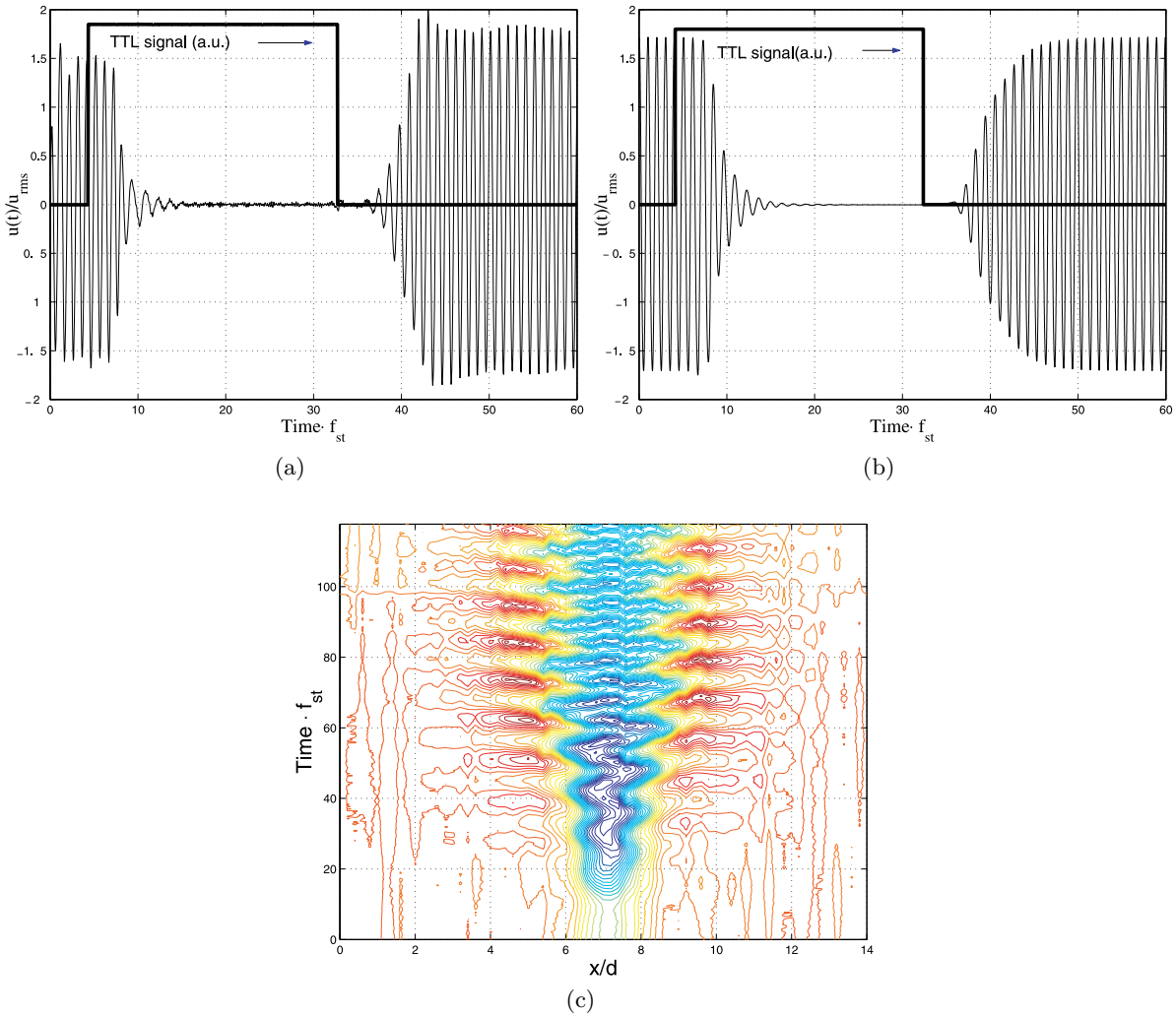

Fig. 8. Comparison of dynamic wake response of the BvK instability forced by an step function for the sink strength. Vortex shedding suppression occurs during the active time of the sinks associated to the high value of the sink step function (denoted here as TTL signal). (a) Experimental velocity signal recorded at $y/d = 18$ and slightly off the cylinder axis, performing an on–off operation of the solenoid valve at $Re = 75$. Characteristic shedding frequency is $f_{st} = 10.7$ Hz. A high local sink rate of $Q = 22$ cm^3/s is used. When normalized by the projected flow rate per unit length $Q_p = v_0 d$, we get $Q/Q_p = 1.9$ (b) Normalized transverse velocity fluctuation obtained from our numerical simulation. We display the centerline wake response at $y/d = 18$, using a normalized sink strength of $Q/Q_p = 1.2$ for a Reynolds number of $Re = 73$, close to the experimental value. (c) Experimental contours of fluid velocity at $y/d = 18$ for $Re = 75$, showing the starting BvK instability.

projected flow rate per unit length, defined by $Q_p = v_0 d$, to compare sink strength between numerical simulations and experiments.

Fluid wake–velocity was measured with a calibrated TSI hot wire probe, 20 μm in diameter and 2 mm long sensitive length, located at $y/d = 13$ from the rear end of the cylinder. It was operated with a constant temperature anemometer developed at our laboratory. Signals delivered by the anemometer were found to be higher in amplitude when the probe is located slightly off the center of the cylinder's wake at $x/d \sim 13$ as it was observed elsewhere [19]. Data signals were acquired with a 250 kHz and 16 bits DT322 Data Translation card on a Pentium machine, previously filtered by a 12 dB/Octave anti-aliasing filter.

Dynamic tests

Dynamic behavior of the control method means that we are looking for the forced response of the BvK instability under a rapid on-off operation of the solenoid valve (TTL step), which furnishes an approximate step function of the local sink strength.

Experimentally speaking, both the TTL step for the valve operation and the velocity signal recording with the hot wire probe, should be synchronous, *i.e.*, started with a common trigger signal. The characteristic experimental wake response is very similar to the numerical one. In Figures 8a, b, we show two fluid velocity signals from experiment and numerical simulations. We show the normalized fluid velocity as a function of non dimensional time in both

cases. Note that the comparison should be qualitative; the single hot wire probe gives us the absolute value of fluid velocity instead of the exact transverse fluid velocity $u(t)$ that we get from the numerical run and because the experiment is in three dimensions whereas the numerical run is in two dimensions. However, the wake's dynamic response is similar. After a few time units from the beginning of the step function, fluid velocity starts to be damped, the BvK instability is being inhibited, which means that fluid velocity fluctuations fall into a background level. Again, when the step is off, after a few time units the BvK instability develops and the fluid velocity recovers its periodic behavior. Note that the two figures show that the damped region and the growing one have different growth rates. The damped mode is always faster, due to the rapid fall off of the valve, than the unstable mode.The spatial extension of the unstable mode can be seen in Figure 8c, where we display a two dimensional contour plot of experimental velocity data. Operating our system as explained above, but performing a synchronized transverse scanning over the overall wake velocity, we get the time evolution of the BvK instability onset, in the form of contours of velocity. The starting BvK instability saturates rapidly, then forming its classical periodic spatial pattern.

From this simple test, we recognize that the control method modifies the characteristic eigen mode associated to the BvK instability. The complex growth rate should involve not only a Reynolds dependence, as it was pointed before, but also a sink strength dependence. The sink strength do modify both the real and imaginary parts of the unstable eigen mode. The imaginary part, associated to the shedding frequency, is reduced with increasing values of Q as shown in the preceding section. The real part, associated to the temporal growth rate of the amplitude of the BvK instability is shifted to the left of the complex plane, resulting in negative growth rates or stable eigen modes, when $Q > Q_c$.

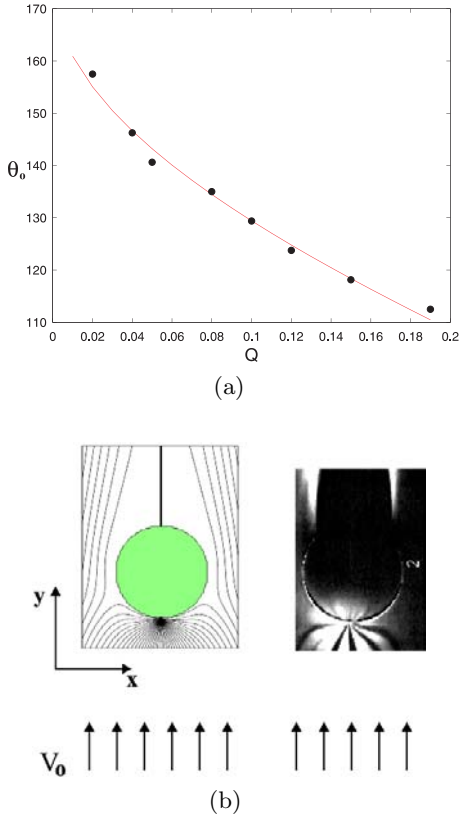

Fig. 9. (a) Comparison of the bifurcation angle θ_o as a function of the sink strength at $Re = 100$ for $0 < Q < 0.2$ (the normalized interval is $0 < Q/Q_p < 3.4$). Discrete values (•) were obtained from our numerical simulation. Continuous curve was obtained from potential theory. (b) Schematic comparison between an experimental smoke wire visualization ($Re = 110$, $Q = 10$ cm^3/s equivalent to $Q/Q_p = 0.6$), and our numerical results at $Re = 100$, $Q = 0.07$ (or $Q/Q_p = 1.2$), in the form of contours lines for the stream function $\Psi(x, y)$ where $\delta\Psi = 0.1$. Remember that θ_o decreases with increasing Q.

Steady state tests

Here we want to compare the local properties of the flow field near the cylinder surface, associated to constant and steady forcing of sink strength Q. As we mentioned before, the sink induces a bifurcation of the original stagnation point into two symmetric ones located at both sides of the cylinder surface.

The angle θ_o predicted from potential theory was compared to the angle found from our numerical runs. From our runs we can find these two bifurcated stagnation points, looking for a local maximum of the surface pressure field $p(r = d/2, \theta)$ for different values of $Q > Q_c$ at $Re = 100$. In Figure 9a we show both the angle θ_o found in our runs and the angle given by our potential solution θ_o, where we found a very close agreement. This indicates that the front region near the cylinder surface before the stagnation points occur, looks like an inviscid region, confirming that the bifurcation mechanism, should be, in some way, responsible of the subsequent vortex shedding suppression. When we look at the front stagnation point in the free case (sink is off), the local pressure $p_f(t)$ changes periodically in time, with a frequency twice the Strouhal frequency. That means a stagnation point which is performing small oscillations around $\theta = \pi$. When the sink is on, this point disappears and we found two symmetric ones at $\pm\theta_o$, imposing a new symmetry on the pressure field around the cylinder. Figure 9b displays both the contours of stream lines of the fluid flow computed from our numerical runs, and a smoke wire image from our experimental flow visualizations.

These two bifurcated stagnation points, observed over both slides, are symmetric with respect to the main flow axis. The fraction of fluid comprised between singular stream lines, is being pumped from the system in both cases.

For the smoke wire image, the situation considers a circular cylinder of diameter $d = 8$ mm, on a uniform fluid flow at $Re = 110$ and individual sink strength is $Q = 10$ cm^3/s. Sink strength when normalized by the projected flow rate per unit length, $Q_p = v_0 d$, gives

$Q/Q_p = 0.6$. The flow imaging method consists of a green laser sheet passing through the near wake (and aligned with the small hole position $d_\epsilon = 0.5$ mm), which receives smoke particles feeded upstream, the scattered light perpendicular to the laser sheet give us the flow image recorded with a ccd camera.

Concluding remarks

Numerical simulations of time varying Navier Stokes equations in a 2D rectangular channel with a cylinder inside, were performed. The characteristic BvK instability onset can be delayed through a recent control method based on the suction of the front stagnation point of the cylinder. Suction was modelled introducing the idea of a local sink of strength Q. When the sink is activated, the BvK instability is damped and vortex shedding is suppressed. Even though there exists a minimum Q, a critical value Q_c from which vortex suppression takes place, this parameter was found to depend on the Reynolds number, such that increased Re numbers needed higher Q_c values for complete vortex suppression. Agreement was found between potential theory and numerical simulations. Qualitative agreement was found on the dynamic and steady state behavior of the forced BvK instability between numerical and experimental results. Applications of this method to high Reynolds number flows, should need an important sink strength to get vortex suppression, however at reasonable sink rates, the characteristic properties of BvK instability will be strongly modified, the shedding frequency reduced, and the unstable modes shifted toward more stable regions of the complex plane. Extension of the numerical method to 3D situations, using particular bluff bodies like airfoils, are part of a current work.

Financial support from FONDECYT (Grant N° 1990571) and Fundación Andes (Grant C-13600/4) are gratefully acknowledged.

References

1. M. Provansal, C. Mathis, L. Boyer, J. Fluid Mech. **182**, 1 (1987)
2. R.H. Hernández, C. Baudet, Europhys. Lett. **49**, 329, (2000)
3. see for instance, G.K. Batchelor, *An Introduction to Fluid Mechanics* (Cambridge University Press, 1967)
4. K. Kwon, H. Choi, Phys. Fluids **8**, 479 (1996)
5. D.S. Park, D.M. Ladd, E.W. Hendricks, Phys. Fluids **6**, 2390 (1994)
6. J.W. Schaeffer, S. Eskinazi, J. Fluid Mech. **6**, 241 (1959)
7. S. Taneda, J. Phys. Soc. Jpn **45**, 1038 (1978)
8. P.T. Tokumaru, P.E. Dimotakis, J. Fluid Mech. **224**, 77 (1991)
9. K. Roussopoulos, J. Fluid Mech. **248**, 267 (1993)
10. R.D. Blevins, J. Fluid Mech. **161**, 217 (1985)
11. P. Huerre, P. Monkewitz, Annu. Rev. Fluid Mech. **22**, 473 (1990)
12. R.H. Hernández, C. Baudet, S. Fauve, Eur. Phys. J. B **14**, 773 (2000)
13. S.V. Patankar, *Numerical Heat Transfer and Fluid Flow* (Hemisphere Publishing Corporation, Washington D.C., 1980)
14. R.H. Hernández, R.L. Frederick, Int. J. Heat Mass Transfer **37**, 411 (1994)
15. R.H. Hernández, Int. J. Heat Mass Transfer **38**, 3035 (1995)
16. A. Pacheco, *Simulación numérica de algoritmos de control de la inestabilidad de Bénard von Kármán*, Tesis de Ingeniero Civil Mecánico, Universidad de Chile, Santiago, Chile, 2001
17. A. Roshko, *On the development of turbulent wakes from vortex streets*, NACA Report, 1191 (1954)
18. M. Gaster, J. Fluid Mech. **38**, 565 (1969)
19. L.S.G. Kovasznay, Proc. R. Soc. Lond. A **198**, 174 (1949)
20. A. Papoulis, *Probability, Random Variables and Stochastic Processes* (McGraw Hill, New York, 1965).
21. C.H.K. Williamson, J. Fluid Mech. **206**, 579 (1989)